Journal of Trace Elements in Medicine and Biology 55 (2019) 154–169

Contents lists available at ScienceDirect

Journal of Trace Elements in Medicine and Biology

journal homepage: www.elsevier.com/locate/jtemb

Biodistribution and toxickinetic variances of chemical and green Copper oxide nanoparticles *in vitro* and *in vivo*

Aditi Dey[a], Subhankar Manna[a], Jaydeep Adhikary[b], Sourav Chattopadhyay[c], Sriparna De[d], Dipankar Chattopadhyay[d,*], Somenath Roy[a,*]

[a] Immunology and Microbiology Laboratory, Department of Human Physiology with Community health, Vidyasagar University, Midnapore, 721102, West Bengal, India
[b] Department of Chemical Sciences, Ariel University, Ariel, 40700, Israel
[c] Molecular Genetics and Therapeutics Lab, Indian Institute of Technology, Kanpur, India
[d] Department of Polymer Science and Technology, USCTA, University of Calcutta, 92 A.P.C road, Kolkata, 700009, West Bengal, India

ARTICLE INFO

Keywords:
Copper oxide nanoparticle
Nanotoxicology
Biochemical toxicity
Biodistribution
Apoptotic protein
Cytokine

ABSTRACT

In this study, chemical (S1) and green (S2) Copper Oxide nanoparticles (NPs) were synthesized to determine their biodistribution and toxicokinetic variances *in vitro* and *in vivo*. Both NPs significantly released Copper ions (Cu) in lymphocytes and were primarily deposited in the mononuclear phagocyte system (MPS) such as the liver and spleen in mice. In particular, S2NPs seemed to be prominently stored in the spleen, whereas the S1NPs were widely stored in more organs including the liver, heart, lungs, kidney and intestine. The circulation in the blood and fecal excretions both showed higher S2NPs contents respectively. Measurements of cell viability, Hemolysis assay, Reactive Oxygen Species (ROS) generation, biochemical estimation and apoptotic or necrotic study in lymphocytes after 24 h and measurements of body and organ weight, serum chemistry evaluation, cytokines level, protein expressions and histopathology of Balb/C mice after 15 days indicated significant toxicity difference between the S1NPs and S2NPs. Our observations proved that the NPs physiochemical properties influence toxicity and Biodistribution profiles *in vitro* and *in vivo*.

1. Introduction

Copper oxide nanoparticles (CuONPs) are extensively used in semiconductor devices, solar energy converter, batteries, microelectronics, gas sensor and heat transfer fluids and are also used in manufacturing processes as industrial catalysts [1,2]. Further, CuONPs have attracted attention in many biomedical applications mostly due to their antimicrobial activity against a wide range of pathogenic microorganisms and cost effective synthesis [3].

Despite its great potential in biomedical applications, toxicity studies of CuONPs reveals its cytotoxic effect in human airway epithelial cells [4] and smooth muscle cells [5] rendered by oxidative stress. CuONPs induced P^{38} has been shown to phosphorylate in mice endothelial cells due to oxidative stress which upregulated the plasminogen activator inhibitor-1 [6] and elicits DNA damage and apoptosis [7]. Furthermore, synthesis of CuONPs by thermal decomposition [8], being involved of toxic chemicals, high temperature and high pressure is responsible for environmental toxicity and in addition is toxic to living systems [9].

To reduce the toxicity towards normal cells, green synthesized CuONPs has surfaced as a biocompatible alternative *prima facie* attributing to its biological accessibility to the target organ through biological barriers [3]. Biogenic synthesis of metal NPs being easy can be produced in a large scale without any contamination and also provides distinct morphology of the particles [10]. Green synthesized CuONPs possesses several advantages and demonstrates better efficacy compared to physical or chemical synthesis method [11,12]. Among various plants, *A. indica*, a traditional medicinal plant which grows mainly in tropical and semi-tropical climates have been found to have versatile applications in medical science [13]. The leaves, flowers, fruits and seeds of *A. indica* have promising chemopreventive and therapeutic properties [14]. It has also been reported that components of *A. indica*

Abbreviations: CuO, Copper oxide; CuONPs, Copper oxide nanoparticles; DLS, Dynamic Light Scattering; RPMI1640, Roswell Park Memorial Institute; DOX, Doxorubicin; H_2DCFDA, 2',7'-Dichlorodihydrofluorescein diacetate; HEPES, N-(2-hydroxyethyl)-piperazine-N- (2-ethanesulfonic acid); LDH, Lactate Dehydrogenase; MTT, 3-[4,5dimethylthiazol- 2-yl] -2,5-diphenil-tetrazolium bromide; NP, Nanoparticles; PBS, Phosphate-Buffered Saline; ROS, Reactive Oxygen Species; SGOT, Serum glutamic oxaloacetic transaminase; XRD, X-ray diffraction; S1, Chemically synthesized CuO; S2, Green synthesized CuO

* Corresponding authors.
E-mail addresses: dipankar.chattopadhyay@gmail.com (D. Chattopadhyay), sroy.vu@hotmail.com (S. Roy).

https://doi.org/10.1016/j.jtemb.2019.06.012
Received 24 November 2018; Received in revised form 6 June 2019; Accepted 17 June 2019

suppress NF-κβ signalling pathways [15].

Van der Waals and electrostatic forces responsible for cellular internalization in Cu^{+2} O ions, facilitate adhesive interaction of the CuONPs with the cell surface, thereby promoting cellular uptake of the NPs [16].

In vitro toxicity of CuONPs depends not on the Cu release in the growth medium but on the NPs direct penetration into cells and subsequent dissolution of NPs, followed by distribution of toxic Cu^{+2} ions into the cytoplasm of cell [17,18].

To our knowledge, detailed report regarding the toxicity and biodistribution of green synthesized CuONPs *in vitro* and *in vivo* has been eluded. Hence, for further practical implementations, it is essential to evaluate the *in vitro* and *in vivo* toxicity of CuONPs and their biodistribution for the purpose of risk comprehension.

In our previously reported study we reported significant anticancer activity of CuONPs from *A. indica*. But its toxic effect on several organs and lymphocytes was not investigated there. Also due to higher toxicity of marketed CuONPs compared to S1NPs, as analyzed in our laboratory, we designed our study to evaluate biodistribution and toxicokinetics using S1NPs and S2NPs synthesized in our laboratory [19,20].

Herein, we conducted a comparative *in vitro* toxicity of S1NPs with S2NPs in human lymphocytes by investigating the Cu ions internalization, biochemical estimation, ROS generation and apoptotic study. In addition, we investigated the *in vivo* toxicity of S1NPs and S2NPs by evaluating biochemical parameters, apoptotic and cytokines estimation and histopathology following 15-day repeated intraperitoneal doses in Balb/C mice.

Further, we investigated body weight, organ weight, organ distribution and excretion to elucidate the primary accumulation sites and elimination routes of S1NPs and S2NPs *in vivo*. In this work, we report for the first time, to the best of our knowledge, the biodistribution and detailed toxicity *in vivo* of S1NPs and S2NPs by conducting a repeated dose toxicity study.

2. Materials and methods

2.1. Chemicals and reagents

Histopaque-1077, Propidium iodide (PI), RNaseA, 3-(4,5-dimethyl-2-thiazolyl)-2,5-diphenyl-2H-tetra-zolium bromide (MTT reagent), NaOH, ethidium bromide and acridine orange were procured from Sigma (St. Louis, MO, USA). Minimum Essential Medium (MEM), RPMI 1640, fetal bovine serum (FBS), penicillin, streptomycin, sodium chloride (NaCl), sodium carbonate (Na_2CO_3), sucrose, ethylene diamine tetra acetate (EDTA) and dimethyl sulfoxide (DMSO) were purchased from Himedia, India. Tris−HCl, Tris buffer, KH_2PO4, K_2HPO4, HCl, formaldehyde, alcohol and all other chemicals of the highest purity grade were procured from Merck Ltd., Mumbai, India.

2.2. Preparation of leaf extracts

Leaves of traditional plant *Azadirachta indica* (*A. indica*) were collected from the campus of the Vidyasagar University (22.4320 °N, 87.2979 °E), West Bengal, India. After 100 g of leaves of *A. indica* were taken and washed gently with double distilled water, the leaves were chopped and dried in a hot air oven. After the completion of the total drying process, these materials were pulverized in a grinder until fine dust and dissolved in distilled water(10 g dust/100 mL distilled water) followed by filtration with Whatman filter paper No.1. The filtrate was collected and freeze-dried and kept at 4 °C temperature for storage.

2.3. Synthesis of S1NPs and S2NPs

2.3.1. Synthesis of S1NPs

A methanolic solution (5 mL) of 2-benzoyl pyridine (0.366 g; 2 mmol) was added dropwise with constant stirring to a methanolic solution (10 mL) of Copper (II) Sulphate pentahydrate (1 mmol; 0.370 g). The stirring was continued for further 0.5 h and then an aqueous solution (5 mL) of sodium dicyanamide (0.178 g; 2 mmol) was added dropwise. After further 1 h stirring, the resulting mixture was filtered and the filtrate was collected. Single crystals suitable for X-ray data collection were obtained from the filtrate after a few days (Yield: 87%). Then the solid compound are crushed well and heated at 620 °C in a furnace for 2 h. The black powder compound was obtained, washed well in methanol and dried and used as S1NPs [20,21].

2.3.2. Synthesis of S2NPs

CuONPs were synthesized from a traditional medicinal plant *A. indica* in accordance with previous protocol [19]. Analytical grade of cupric sulphate (5 mM) 90 mL solution, prepared by deionized water was mixed with 20 mL of filtrate obtained previously in a magnetic stirrer at 60 °C temperature. The mixture was kept at room temperature. Gradually a brownish black precipitate was observed at the bottom of the conical flask. Then it was dried and kept in storage for further use as S2NPs.

2.4. Characterization

To know the surface chemistry of S1NPs and S2NPs, FT-IR spectroscopy was carried out with a Perkin 118 Elmer FT-IR spectrometer (Spectrum Two FT-IR spectrometer, 119 Version: 10.03.07.01120) in compliance with Mohapatra et al. [22]. Here, 1 mg mass of both S1NPs and S2NPs were mixed with 100 mg KBr medium separately to prepare a thin film under atmospheric pressure. The FT-IR spectra were obtained in between 500-4000cm^{-1}.

The hydrodynamic sizes of S1NPs and S2NPs and zeta potential were measured by DLS (Dynamic Light Scattering) using a Zetasizer-Nano ZS (Malvern, Malvern Hills, U.K.) as previously described [23]. NPs of 100 μg/mL concentration each, were sonicated for 2 min and two drops of aqueous suspension of NPs were suspended separately in both 10 ml of Millipore water to measure the hydrodynamic sizes. Similarly hydrodynamic sizes were measured using PBS suspension of NPs. The experiments were triplicated to obtain average size of NPs.

The morphology and surface structures of S1NPs and S2NPs were analyzed using a JEOL (Japan) 3010 high-resolution scanning electron microscope operating at 200 kV. In brief, S1NPs and S2NPs were suspended in deionized water at 1 mg/mL concentration separately, and subsequently sonicated using a sonicator bath until a homogeneous suspension is formed. Sonicated stock solutions of both NPs (0.5 mg/mL) were diluted 20 times, for size measurement. To characterize the size and the shape of the NPs, scanning electron microscopy images were obtained after placing a drop of aqueous NPs suspension onto a glass plate and coated with gold and images were taken [23].

In Ion dissolution study, S1NPs and S2NPs of highest concentrations (100 μg/mL) were suspended in a RPMI 1640 media without FBS and antibiotic for 1 week at 37 °C. The supernatant thus obtained, was used to determine the free Cu ions in the medium through atomic absorption study (AAS) [23]. Here $CuSO_4$ was used as a standard at varied concentrations.

The EDX and XRD study has been performed according to Majumdar et al. [24] and Das et al. [25,26], respectively.

2.5. Selection of human subjects and isolation of peripheral blood lymphocytes

Lymphocytes of six healthy human subjects devoid of any hereditary disease, chronic disease, drug addiction and medications were obtained. The human subjects belonged to the same geographical area and underwent regular routine checkup. The study protocol, approved by the Ethical committee of Vidyasagar University (Approval No. IEC/6-20(Mod)/C-10/16) was in agreement with the declaration of Helsinki, as also previously reported from our laboratory [27].

In compliance with Hudson and Hay [28] blood samples were collected from six healthy human subjects in 5 mL heparin coated vacutainers using veni-puncture method. After diluting 5 mL blood 1:1 with phosphate buffered saline (PBS), Histopaque 1077 (Sigma) was used for density gradient centrifugation at 400Xg (1500 rpm) for 40 min at room temperature using a Pasteur pipette. Lymphocytes comprising the upper monolayer of buffy coat were collected using a clean centrifuge tube and washed thrice in balanced salt solution. Supplemented with 10% FBS, the peripheral blood lymphocytes (PBL) were re-suspended in RPMI complete media and incubated for 24 h in a 95% air 5% CO_2 atmosphere at 37 °C in CO_2 incubator.

2.6. Cell culture

Normal lymphocytes were cultured in a RPMI 1640 complete medium with 10% FBS, 2 mM/L glutamine, 100U/mL penicillin, 100 µg/mL streptomycin under 5% CO_2 and 95% humidified atmosphere at 37 °C in CO_2 incubator.

2.7. Drug preparation

Drug was prepared by making suspension of 10 mg of S1NPs, S2NPs and Doxorubicin (DOX) in PBS. The working concentration (1, 5, 10, 25, 50 and 100 µg/mL) of the drug was prepared by diluting the stock solution with PBS.

2.8. Toxicity in vitro

2.8.1. Toxicity of lymphocytes and RBC

Normal human lymphocytes (2×10^5 numbers of cells in each group) were seeded into 96 wells of tissue culture plate and, after adding Doxorubicin and NPs (S1NPs and/or S2NPs) to the cells at varied concentrations (1, 5, 10, 25, 50 and l00 µg/mL), were incubated for 24 h at 37 °C in a humidified incubator (NBS) maintained with 5% CO_2. The cell viability was estimated by 3-(4,5-dimethyl-thiazol)-2-diphenyltetrazolium bromide (MTT) as previously reported [23].

RBC toxicity was estimated through hemolysis assay as previously reported [23]. 5 mL of EDTA-stabilized human blood samples obtained from healthy subjects were added to 10 mL of PBS, followed by centrifugation at 2200 rpm for 10 min to obtain RBCs. After washing five times with 10 mL of PBS solution, the purified RBCs were diluted to 50 mL with PBS. For the positive control supernatant, the absorption spectrum was in the range of 0.50-0.55 optical density units. For the positive and negative controls, RBCs were incubated with deionized water and PBS and 0.2 mL of diluted RBC suspension obtained was mixed gently with 0.8 mL of S1NPs and/or S2NPs solutions at varied concentrations. The mixtures were kept at room temperature for 3 h, centrifuged at 10,000 rpm for 3 min, and subsequently 100 mL of supernatant from all samples was transferred to a 96-well plate. Here the absorbance values of the supernatants at 570 nm were estimated using an ELISA microplate reader (Bio-rad, India) with the absorbance at 655 nm as a standard. The percent hemolysis of RBCs was determined using the following formula:

Percent of hemolysis = (sample absorbance - negative control absorbance)/ (positive control absorbance - negative control absorbance) x 100

2.8.2. Intracellular concentration of NPs

The concentrations of Cu ions inside the cells were estimated by AAS. Here lymphocytes were treated with 100 µg/mL dose of both S1NPs and S2NPs for different durations (0, 12, 24 and 48 h). Subsequently, lymphocytes were washed with PBS and resuspended in 6 M nitric acid, followed by incubation at 95 °C temperature for 24 h. Acid digested samples were used for the measurement of Cu ions inside the cells using Shimadzu AA-7000 atomic absorption spectroscopy in RPMI 1640 medium as previously reported [23].

2.8.3. Biochemical toxicity markers

After the isolation from the blood, the lymphocytes of different groups pre-warmed in Krebs ringer buffer (KRB) with 10 mM glucose at 37 °C for 3 min and phorbol 12-myristate 13-acetate (PMA) (1 µg/mL) pre-warmed at 37 °C for 5 min were added and the reaction was terminated by placing in ice. After centrifugation for 5 min at 400 *g*, the resultant pellet was resuspended in 0.34 M sucrose, lysed with hypotonic lysis buffer and subsequently centrifugation was carried out at 800 *g* for 10 min. The supernatant thus obtained was used to determine enzyme activity. The NADPH oxidase activity was evaluated spectrophotometrically by measuring cytochrome c reduction at 550 nm. The reaction mixture contained 100 mM NaCl, 10 mM phosphate buffer (pH 7.2), 1 mM $MgCl_2$, 2 mM NaN_3, 80 mM cytochrome c and 100 µl of supernatant (final volume 1 mL). Lastly a suitable amount of NADPH (10–20 µl) was given to initiate the reaction [29].

Lactate Dehydrogenase (LDH) assay was estimated using a sandwich ELISA Kit (Tulip, Mumbai, India) and expressed as mg/dl. After the treatment schedule, 50 µL cell supernatant was used for LDH measurement as per the detailed instructions of the manufacturer.

From the supernatant of cell lysate, lipid peroxidation level was estimated as the concentration of thiobarbituric acid reactive product malondialdehyde (MDA). 100 µl cell supernatant and 100 µl double distilled water were added to 50 µl of 8.1% sodium dodecyl sulfate (SDS) and subsequently incubated for 10 min at room temperature. 375 µl of both 20% acetic acid (p^H 3.5) and thiobarbituric acid (0.6%) were added to the tissue solution and placed in a boiling water bath for 1 h. After boiling, 250 µl of double distilled water along with 1.25 mL of 15:1 butanol–pyridine solution were added to the mixture and subsequently centrifuged at 2000 *g* for 5 min. The supernatant was removed and MDA concentrations were measured spectrophotometrically at 530 nm using Hitachi U-2000 spectrophotometer. The MDA levels were expressed as nmol/mg protein [30].

Nitric Oxide (NO) release assay was performed in accordance with Chakraborty et al. [31]. NO values were expressed as µM/mg protein.

2.8.4. Intracellular ROS generation and Apoptotic or necrotic event analysis

Intracellular ROS estimation was performed using 2,7-dichlorofluorescein diacetate (DCFH2-DA) as previously reported using fluorescence microscopy (Nikon ECLIPSE LV100POL). The DCFH2-DA after passively entering the cell reacts with ROS for the formation of the highly fluorescent compound dichlorofluorescein (DCF). A 100 µM working solution was prepared by diluting 10 mM DCFH2-DA stock solution (in methanol) in culture medium without serum. After the treatment with both NPs for 24 h, cells were washed twice with PBS, incubated in 1.5 mL of working solution of DCFH2-DA at 37 °C for 30 min, lysed in alkaline solution and centrifuged at 2200 rpm. Fluorescence was measured by transferring a 1 mL supernatant to a cuvette at 520 nm emission and 485 nm excitation using a fluorescence spectrophotometer (HitachiF-7000, Singapore). The values were expressed in terms of percent of fluorescence intensity relative to the control wells [23].

Cellular morphology was visualized using ethidium bromide (EtBr) in combination with acridine orange (AO) staining by EtBr/AO double staining. Etbr/AO double staining is a vital process for investigating the toxicity of S1NPs and S2NPs. Here Etbr stains the nuclear changes and AO is used to detect the apoptotic body formation inside the cytoplasm. Upon using both EtBr and AO together, green color obtained indicates living cells, whereas orange and red color indicates late apoptosis and necrosis respectively. After treatment of cells with S1NPs and S2NPs, the lymphocytes (2×10^5cells/mL) were washed with cold PBS and then stained solution of PBS containing EtBr and AO (50 µg/mL; Vol/Vol) at room temperature for 5 min. Subsequently, the cells were washed thrice with PBS, and images of the stained cells were observed under fluorescence microscope (NIKON ECLIPSE LV100POL) at 400X magnification [25,26]. In our study, late apoptosis was prominently observed in lymphocytes at higher doses for both NPs.

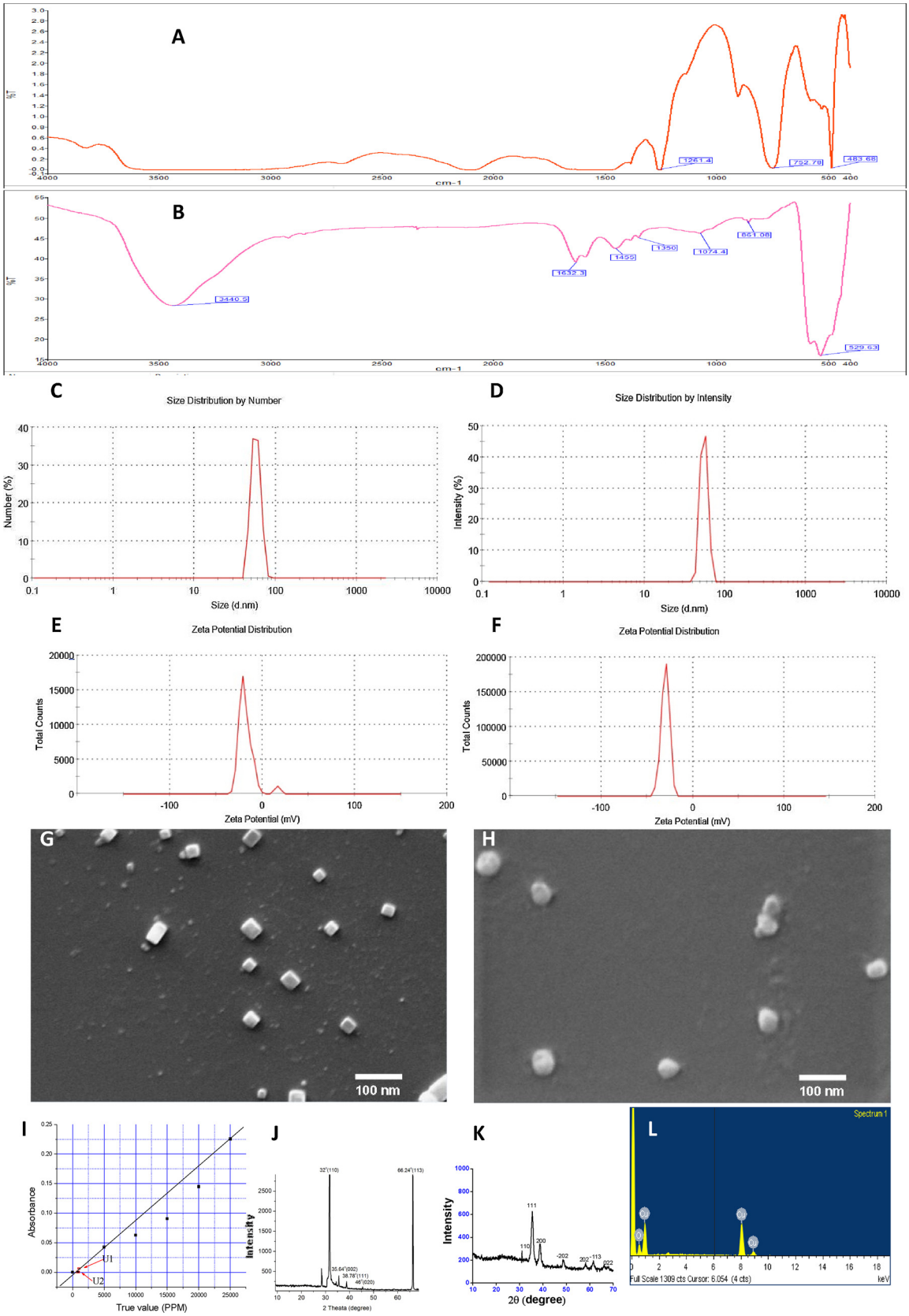

Fig. 1. Physical characterization of S1NPs and S2NPs. FT-IR spectroscopy of **(A)** S2NPs and **(B)** S1NPs. Hydrodynamic size measurement of **(C)** S1NPs and **(D)** S2NPs by DLS in PBS. Surface zeta potential measurement of **(E)** S1NPs and **(F)** S2NPs in PBS. Size measurement of **(G)** S1NPs and **(H)** S2NPs by SEM study. **(I)** Dissolution study of S1NPs (U1) and S2NPs (U2) at a dose of 100 μg/mL dose. Released concentration of Cu ions was estimated by AAS. (J,**K)** XRD study of (J) S1NPS and **(K)** S2NPS. **(L)** EDX study of S1NPs.

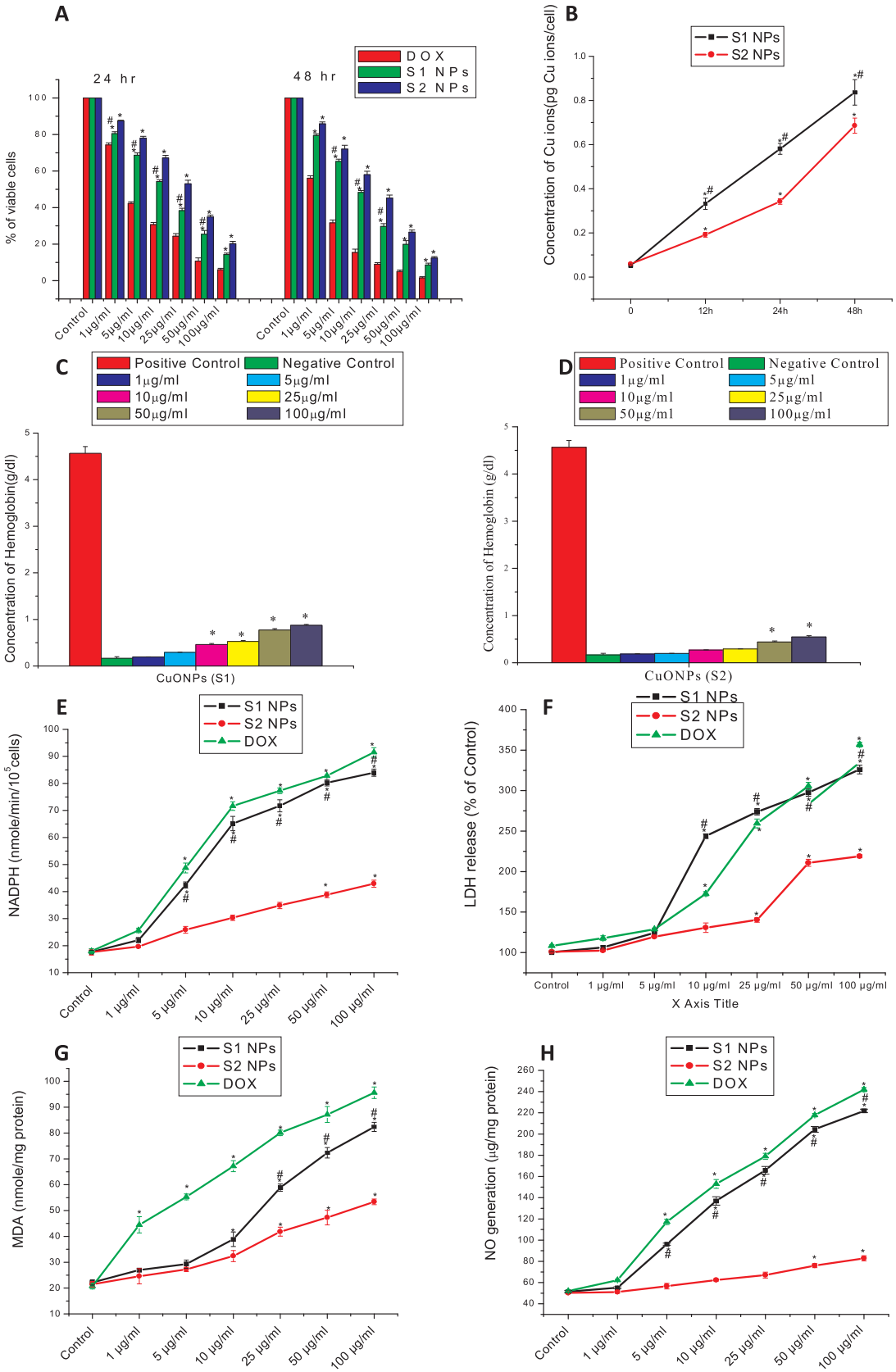

Fig. 2. Cell viability, Intracellular concentration, Hemolysis and Biochemical assay. **(A)** Dose and duration dependent percentage of Lymphocytes death by S1NPs, S2NPs and DOX was estimated by MTT assay. Values were expressed as mean ± SEM. Superscripts indicated a significant difference as ($P < 0.05$) compared with control. **(B)** Estimation of Cu ions concentration from S1NPs and S2NPs inside the lymphocytes at different time duration by AAS. **(C, D)** Estimation of hemolysis after **(C)** S1NPs and **(D)** S2NPs exposure for 24 h. **(E–H)** Estimation of **(E)** NADPH oxidase level, **(F)** LDH level, **(G)** MDA enzymatic level and **(H)** NO levels from lymphocytes after treatment with S1NPs, S2NPs and DOX for 24h. Values are expressed as mean ± SEM of three experiments; *superscripts indicate significant differences ($P < 0.05$) compared with the control group and #superscripts indicate significant differences of S1 NPs compared to S2 NPs.

Table 1
Represents the change indifferent biochemical toxicity markers (NADPH, Nitric Oxide, MDA and LDH) after treatment with S1NPs and S2NPs with different doses (1–100 μg/ml). Values were expressed as a change in fold compared to control.

Toxicity Markers	Different Doses(μg/ml) Values expressed as Fold Change					
	1	5	10	25	50	100
NADPH (S1)	1.24	2.40	3.68	4.05	4.54	4.75
NADPH (S2)	1.11	1.46	1.72	1.98	2.20	2.43
Nitric Oxide (S1)	1.07	1.86	2.66	3.22	3.97	4.31
Nitric Oxide (S2)	1.01	1.12	1.24	1.33	1.51	1.65
MDA (S1)	1.21	1.32	1.75	2.65	3.26	3.71
MDA (S2)	1.14	1.26	1.50	1.94	2.20	2.48
LDH (S1)	1.05	1.23	2.42	2.72	2.96	3.25
LDH (S2)	1.01	1.19	1.30	1.40	2.10	2.18

2.8.5. Cytokines analysis and Pro and Anti-apoptotic marker analysis

Cytokines including pro-inflammatory (TNF-α) and anti-inflammatory (IL-10) were measured using ELISA assay kit (Enzyme linked immunosorbent assay). Pre coated plates of Human TNF-α ELISA Ready-SET-Go, E-bioscience, India were used in accord with manufacturer's instruction. The sensitivity limit of the cytokines was 4.0 pg/mL and 2.0 pg/mL for TNF-α and IL-10, respectively. The concentrations of the cytokines were expressed as pg/mL/10^6 cells.

The level of pro-apoptotic factors (Caspase-8, Caspase-3, p38 and Caspase-9) and anti-apoptotic factors (pAKT and Bcl2) were estimated using an ELISA [32]. Optical densities were determined at 450 nm using an ELISA reader (BioRad) and all the experiments were performed thrice.

Here cell free supernant of lymphocytes were used as positive control.

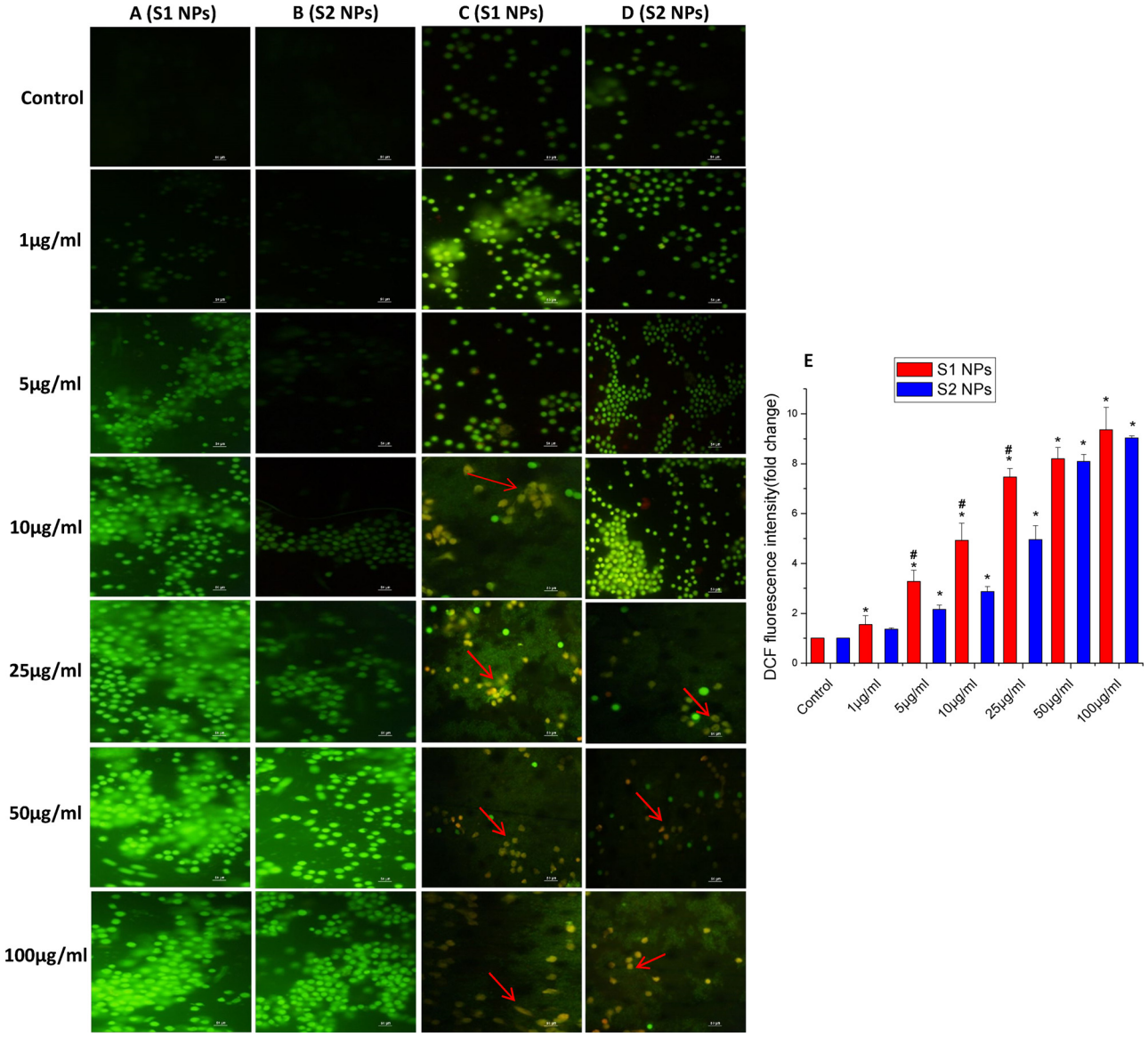

Fig. 3. Fluorescence microscopic images of ROS and Apoptotic phenomenon of human lymphocytes. **(A,B)** Effect of **(A)** S1NPs and **(B)** S2NPs on lymphocytes were visualized under fluorescence microscope by DCHF2DA staining with different doses. **(C,D)** Apoptotic or necrotic event of **(C)** S1NPs and **(D)** S2NPs on lymphocytes were visualized under fluorescence microscope by Etbr/AO double staining with different doses with original magnification of 400 × . **(E)** Fluorescence intensity of DCF measured at 485nm excitation and 520nm emission using a fluorescence spectrophotometer. Intensity of control cells was set to 1.00. Data is represented as the fold change of the ROS level in the control group. Values are expressed as mean ± SEM of three experiments; *superscripts indicate significant difference ($P < 0.05$) compared with the control group and #superscripts indicate significant differences of S1 NPs compared to S2 NPs.

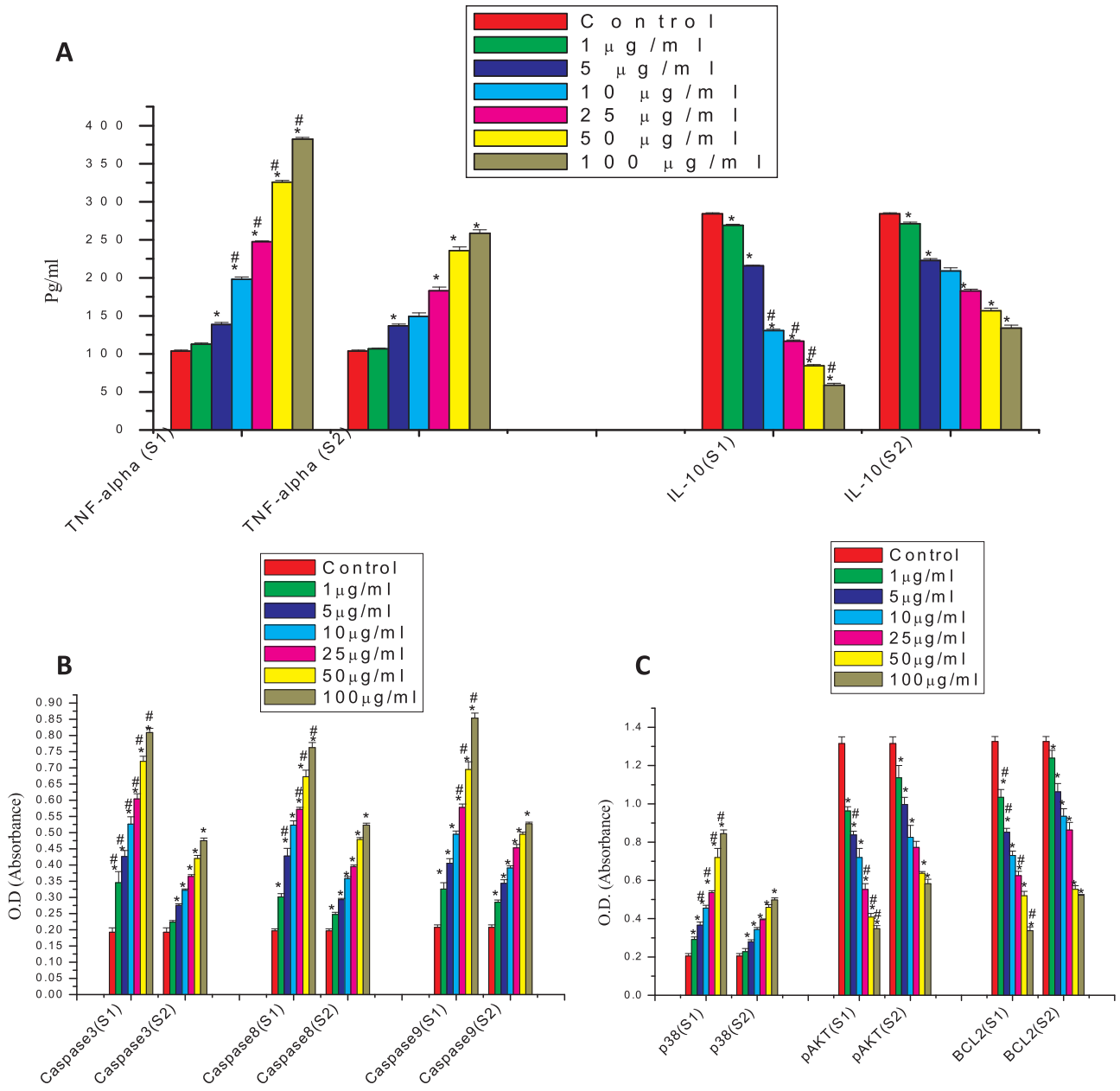

Fig. 4. Cytokines and Apoptotic markers analysis *in vitro*. **(A)** Pro and anti-inflammatory response of S1NPs and S2NPs on lymphocytes after 24 h treatment (TNF-α, IL-10). **(B,C)** Alteration of pro – apoptotic (Caspase – 8, Caspase – 9, Caspase – 3, p38) and anti – apoptotic (pAKT, Bcl2) response of S1NPs and S2NPs. Values are expressed as mean ± SEM of three experiments; *superscripts indicate significant differences ($P < 0.05$) compared with the control group and #superscripts indicate significant differences of S1 NPs compared to S2 NPs.

2.9. *In vivo toxicity assessment*

Female Balb/C mice of 6–8 weeks old, within the range of 25–35 g weight were taken for the experiment. The animals were fed a standard vitamin rich pellet diet with water given *ad libitum*, and were housed in a polypropylene cage (Terson) in the departmental animal house with a 12 h light & dark cycle under room temperature. Here animals were maintained according to the guidelines of the National Institute of Nutrition, Hyderabad, India and Indian Council of Medical Research and approved by the ethical committee of Vidyasagar University (approval no IEC/6-10(Mod)/C-9/16). Balb/C mice were divided into five groups, containing six mice each. After S1NPs and S2NPs were suspended in a PBS solution of p^H 7.4, both NPs were ultra sonicated for 10 min and subsequently injected intraperitoneally with 100, 200, 500 and 1000 µg/kg Body weight doses. Here mice were injected at every 3 days interval for 15 days [23].

2.9.1. *Assessment of serum chemistry*

Blood sample of the Balb/C mice was kept at room temperature for 2 h, followed by centrifugation at 850 g for 15 min. Using the serum obtained LDH, SGOT and creatinine levels were ascertained according to the kit manufacturer's instruction.

2.9.2. *Quantitative analysis of S1NPs and S2NPs in tissues*

Approximately 0.1-0.5 g tissue (Liver, Lungs, Kidney, Spleen, Heart, Intestine and feces) and approximately 0.3 mL of blood sample were allocated to determine the amount of Cu ions of S1NPs and S2NPs using AAS [33]. The samples were dissolved in 12 mL digestion solution (HNO_3:$HClO_4$ = 5:1), heated to 230 °C and when the reaction reached equilibrium, the temperature was increased to 280 °C. For NPs

Table 2
Represents the change in different pro and anti-apoptotic markers level after the treatment with S1NPs and S2NPs with different doses (1–100 μg/mL) on lymphocytes. Values were expressed as a change in fold compared to control.

Apoptotic Markers	Different Doses (μg/ml). Values Expressed as Fold change					
	1	5	10	25	50	100
Caspase 3(S1)	1.78	2.12	2.73	3.52	3.78	4.21
Caspase 8 (S1)	1.52	2.16	2.65	2.89	3.41	3.86
Caspase 9 (S1)	1.57	1.95	2.39	2.78	3.35	4.12
P38 (S1)	1.42	1.78	2.23	2.62	3.52	4.13
pAKT (S1)	1.36	1.57	1.82	2.38	3.22	3.77
Bcl2 (S1)	1.28	1.55	1.81	2.12	2.55	3.93
Caspase 3(S2)	1.29	1.61	1.89	2.14	2.47	2.79
Caspase 8 (S2)	1.39	1.64	2.02	2.22	2.70	2.95
Caspase 9 (S2)	1.54	1.85	2.11	2.44	2.67	2.84
P38 (S2)	1.27	1.56	1.92	2.21	2.57	2.79
pAKT (S2)	1.15	1.25	1.39	1.55	2.24	2.40
Bcl2 (S2)	1.30	1.48	1.76	1.91	2.07	2.20

treatment group, after removal from the heating block, the digested organ samples were diluted to 25 mL with Milli-Q water to determine the Cu concentrations with AAS.

2.9.3. Estimation of cytokines level and Pro and anti-apoptotic markers analysis from Serum

Cytokines estimation and Apoptotic markers estimation were performed according to above mentioned method of section 2.8.5. Here serum of Control mice has been used as a positive control.

2.9.4. Histopathological study of tissues

Tissues were fixed in 10% formalin, followed by embedding in paraffin. Subsequently, 5 μm thick paraffin section was obtained and stained with hematoxylin and eosin.

2.10. Estimation of protein

Protein content was analyzed from cell free supernatant of lymphocytes. Protein estimation was performed in accordance with Lowry et al. [34].

2.11. Statistical analysis

All the data were expressed as mean ± SEM, n = 6. Comparisons between the means of control and treated groups were made by one-way ANOVA test (using a statistical package, Origin 6.1, North-ampton, MA 01060, USA) with multiple comparison t-tests, $p < 0.05$ as a limit of significance.

3. Results

3.1. Physical characterization of the NPs

From the FT-IR study of S1NPs (Fig. 1**b**), metal-oxygen vibration and aromatic C–H stretching frequency were observed through characteristic peaks in the range of 483.68 cm^{-1} and 752.78 cm^{-1} respectively. In S2NPs (Fig. 1**a**), characteristic peaks of metal-oxygen vibration (529.63 cm^{-1}), C–O stretching vibration (1030-1110 cm^{-1}) [35], phenolic OH (3200-3500 cm^{-1}) [36] were observed. As shown in Fig. 1**c-d**, S1NPs exhibited rectangular shape with diameter 24 ± 6 nm, while S2NPs showed spherical shape with diameter 44 ± 9 nm. The mean hydrodynamic diameter (HD) of S1NPs and S2NPs were 52 ± 3 nm (Fig. 1**c**) and 61 ± 6 nm (Fig. 1**d**), which were larger than the corresponding sizes from SEM measurements. The stability and agglomeration rate of S1NPs and S2NPs were evaluated from the negative zeta potential (-18.9mv and -30.0mv) (Fig. 1**e-f**) and polydispersity index (0.410 and 0.359) respectively. Similar zeta potential result was observed by Yugandhar et al. [36]. The purity and crystalline structure of S1NPs and S2NPs were measured by EDX and XRD pattern respectively. EDX of S1NPs (Fig. 1**i**) shows elemental presence of Cu and Oxygen and elemental presence of S2NPs was previously reported from our laboratory [19]. XRD patterns of S1NPs (Fig. 1***j***) synthesized by chemical method shows noticeable peaks at 2θ values of 32°, 35.64°, 38.78°,46°, 53.5°, 58.2°, 66.24° for the respectively marked indices of (110), (002), (111), (020), (113) respectively [37]. The XRD patterns of the S2NPs (Fig. 1**k**) showed similar diffraction peaks without considerable shift in the peak position [35]. It can be visualized that all the peaks of S2NPs are well coordinated with the diffraction pattern of monoclinic crystal structure. The distinct CuO reflections observed in the XRD patterns indicates the high crystallinity of the synthesized S2NPs.

As shown in Fig. 1g, Cu ions dissolution rates were 933PPM and 728PPM for S1NPs and S2NPs respectively at 100 μg/mL dosage.

3.2. In vitro study

3.2.1. Cell viability of lymphocytes

As shown in Fig. 2a, both S1NPs and S2NPs significantly reduced lymphocytes at both time points compared to the control. Percentages of cell death increased likewise with increment in doses (1–100 μg/mL) for both NPs. However, after 24 h, percentages of cell death in S1NPs treated lymphocytes (19.57%, 31.34%, 45.77%, 61.64%, 74.54% and 85.69%) were significantly higher compared to control than that of S2NPs treated lymphocytes (12.56%, 21.94%, 32.82%, 47.00%, 65.11% and 79.77%) at similar doses. Additionally, DOX killed lymphocytes by 25.71%, 57.74%, 69.3%, 75.69%, 89.30% and 94.03% compared to control after 24 h. After 48 h the % of cell death increased in case of both NPs and DOX in a dose dependent manner. But S1NPs killed lymphocytes more than S2NPs which indicate more toxic effect on lymphocytes. Hence on the basis of % of cell death, 24 h was taken into consideration for further treatment although it was also toxic but less than 48 h.

3.2.2. Intracellular concentration of NPs in lymphocytes

As shown in Fig. 2b, intracellular concentration of S1NPs and S2NPs for varied time points at 100 μg/mL dose was observed. After 24 h, the Cu ions concentration in S1NPs treated lymphocytes (0.58 pg ions/cell) was significantly higher than S2NPs treated lymphocytes (0.34 pg ions/cell).

3.2.3. Hemolysis assay

The hemolytic activity of S1NPs and S2NPs exhibited increasing trends with increase in doses from 10 to 100 μg/mL and 50–100 μg/mL respectively compared to the negative control after 24 h. Though, notably the hemolytic activity of S1NPs (0.46, 0.52, 0.77 and 0.87 g/dl) (Fig. 2**c**) was significantly higher compared to control than that of S2NPs (0.270, 0.292, 0.44 and 0.547 g/dl) for 10–100 μg/mL (Fig. 2**d**).

3.2.4. Biochemical assessment of toxicity in lymphocytes

All the toxicity markers estimated from the cell lysate of DOX, S1NPs and S2NPs treated groups displayed increasing trends with gradual increase in dosages (1–100 μg/mL) compared to control. As shown in Fig. 2e, the NADPH oxidase activity of S1NPs (1.24, 2.40, 3.68, 4.05, 4.54, 4.75 folds) was significantly higher compared to control than that of S2NPs (1.11, 1.46, 1.72, 1.98, 2.20, 2.43 folds) at similar doses. Similarly S1NPs displayed higher MDA levels (shown in Fig. 2g) compared to control than that of S2NPs at all respective doses. Note that (shown in Fig. 2**f** and **h**) LDH and NO generation levels of S1NPs were significantly higher than that of S2NPs for doses 10–100 μg/mL and 5–100 μg/mL respectively. The total fold changes were detailed in Table1.

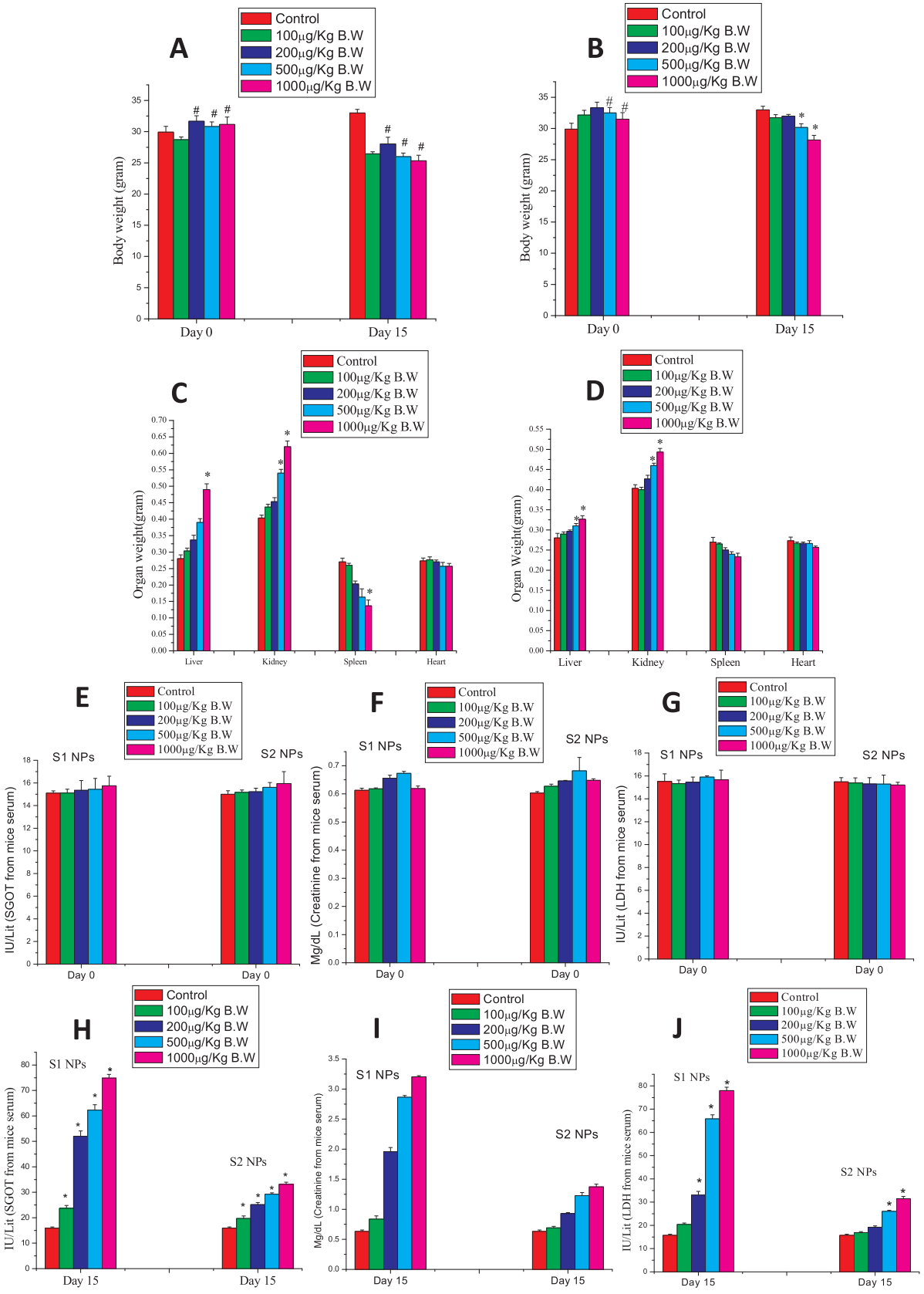

Fig. 5. Estimation of body weight, organ weight and biochemical analysis from animal serum. **(A,B)** Estimation of body weight of **(A)** S1NPs and **(B)** S2NPs treated groups for 15 days. **(C,D)** Estimation of organ weight of **(C)** S1NPs and **(D)** S2NPs treated groups for 15 days. **(E–G)** Estimation of **(E,H)** SGOT, **(F,I)** Creatinine and **(G,J)** LDH levels from the serum of Balb/c mice after the treatment with S1NPs and S2NPs for 0 days and 15 days. Values are expressed as mean ± SEM; *superscripts indicate significant differences ($P < 0.05$) compared with the control group.

Table 3
Estimation of changes in biochemical markers (LDH, SGOT, Creatinine) from mice serum after treatment with S1NPs and S2NPs at different doses (100, 200, 500 and 1000 μg/Kg body weight) for 15 days. Values were expressed as a change in fold compared to control.

Biochemical Markers from Mice serum	15 Days Different Doses(μg/Kg body weight)			
	100	200	500	1000
LDH(S1)	1.29	2.10	4.19	4.96
LDH (S2)	1.10	1.25	1.65	2.00
SGOT (S1)	1.49	3.27	3.91	4.71
SGOT (S2)	1.28	1.63	1.90	2.16
Creatinine (S1)	1.32	3.09	4.51	5.05
Creatinine (S2)	1.17	1.57	2.07	2.32

3.2.5. ROS generation and Apoptotic or necrotic event analysis in Lymphocytes

As shown in Fig. 3**(a–b),** both S1NPs and S2NPs induced lymphocytes, displayed significant amount of ROS generation after 24 h. Note that S1NPs showed increase in ROS generation gradually from initial to higher doses whereas S2NPs showed significant ROS generation only at higher doses (25–100 μg/mL). Also at higher doses (25–100 μg/mL), S1NPs displayed higher ROS generation compared to S2NPs, indicating higher oxidative stress of S1NPs. From the Fig. 3e, the intensity of DCF fluorescence was expressed in terms of ROS production.

Etbr/AO double staining to visualize apoptotic or necrotic event in lymphocytes was performed.

From Fig. 3**(c–d),** we observed significant apoptotic phenomenon in case of both the S1NPs and S2NPs. S1NPs exhibited apoptotic event from 5 to 100 μg/mL doses, whereas S2NPs displayed significant apoptosis from 25 to 100 μg/mL doses. But notably S1NPs displayed more late apoptosis and degradation of lymphocytes shape compared to S2NPs. Note that both NPs did not exhibit necrosis in lymphocytes.

3.2.6. Cytokines and apoptotic markers analysis in lymphocytes

The pro inflammatory cytokine TNF-α level and anti- inflammatory cytokine IL-10 were altered significantly after S1NPs and S2NPs exposure in a dose-dependent manner (1–100 μg/mL) compared to the control. S1NPs and S2NPs increased TNF-α levels by 1.08, 1.34, 1.91, 2.38, 3.14 and 3.68 folds and 1.03, 1.33, 1.45, 1.78, 2.29, 2.51 folds respectively. Contrarily anti- inflammatory cytokine IL-10 levels decreased 1.05, 1.31, 2.17, 2.43, 3.36, 4.83 folds and 1.03, 1.25, 1.33, 1.53, 1.78, 2.09 folds after treatment with S1NPs and S2NPs respectively **(**Fig.4**a)**.

Changes in pro and anti-apoptotic protein levels were estimated compared to the control group from cell lysate using ELISA procedure. As shown in Fig. 4**b-c,** the pro-apoptotic proteins (Caspase-3, Caspase-8, Caspase-9, p38) levels were up-regulated, whereas the anti-apoptotic proteins (pAKT, Bcl2) expression levels were down-regulated after treatment with S1NPs and S2NPs with gradual increase in doses. However the pro-apoptotic proteins level increment in S1NPs was significantly higher compared to S2NPs at all respective dosages. The changes in protein expression levels were enumerated in Table 2, expressed in folds.

3.3. In vivo effects

3.3.1. Effects on body weight and organ weight

The body weight and organ weight of each animal were evaluated after 15 days of treatment through i.p route at different dosages (100, 200, 500 and 1000 μg/Kg) of bodyweight. As shown in Fig. 5a, after 15 days, mice bodyweight of S1NPs treated group depleted significantly compared to the control group at all doses, suggesting toxicity of S1NPs. By contrast, bodyweight decreased in S2NPs experimental groups only at high doses (500–1000 μg/Kg bodyweight) compared to control (Fig. 5b**)**. In Fig. 5**c-d**, liver and kidney of both experimental groups displayed similar upward trends in mass with increase in dosages (100–1000 μg/Kg body weight) compared to control after 15 days. However, the increase in liver and kidney weight of S1NPs treated groups were considerably higher than those of S2NPs treated groups. The spleen weight (Fig. 5c-d) reduced significantly with increase in dosages compared to the control in both S1NPs and S2NPs treated mice, but the reduction was considerably higher in S1NPs treated groups. Organ weight changes are a significant indicator in toxicity studies. From our result, we assume that both S1NPs and S2NPs exert toxic effects against liver, spleen and kidney. In heart, no significant changes in weight were observed in case of both experimental groups compared to the control.

3.3.2. Serum chemistry

Elevated LDH levels of serum were observed for dosages of 100–1000 μg/Kg body weight in case of both S1NPs and S2NPs **(**Fig. 5*j***)**. Furthermore, increment in SGOT and creatinine levels were also noted (Fig. 5**h-i**), thus indicating dysfunction of liver and kidneys. From Fig. 5**h-j**, the values of LDH, SGOT and Creatinine were expressed in Table 3.

3.3.3. Biodistribution and elimination of S1NPs and S2NPs

As shown in (Fig. 6**a-c)**, S1NPs and S2NPs were both accumulated in the liver and spleen, followed by the kidney, lungs, heart and intestine at the highest dosage of 1000 μg/Kg body weight after 15 days. After 15 days S1NPs treated mice and S2 NPs treated mice showed 5.74 fold and 2.74 fold of Cu ions accumulated in liver compared to the control group. Similarly significant amount of accumulation in spleen was also observed compared to the control group. The S2NPs concentrations were significantly 2.02 folds (1 day) and 2.42 folds (15 days) lower compared to S1NPs concentrations in the liver, and in the spleen S2NPs concentrations were significantly 1.95 folds (1 day) and 1.14 folds (15 days) higher compared to S1NPs concentrations (Fig. 6**a-b)**. However, concentrations of S1NPs showed 2.75 folds and 3.8 folds higher levels in the kidney compared with S2NPs (Fig. 6**c)** at both time points. Moreover, concentrations of S1NPs were also significantly higher than the concentrations of S2NPs in the lungs, heart and intestine at both time points (Fig. 6c).

The kinetics of S1NPs and/or S2NPs in the blood and feces was determined by measuring the S1NPs or S2NPs concentrations in successively collected samples at highest dose of 1000 μg/Kg body weight. Fig. 6**d** displayed 1.13 folds and 1.34 folds higher concentrations of S2NPs in blood compared to S2NPs at both time points. As shown in Fig. 6e, the elimination rate of S2NPs in the feces of mice were 2.77 folds and 4.25 folds higher compared to S1NPs.

3.3.4. Cytokines and apoptotic markers analysis

Pro and anti-inflammatory cytokines levels were estimated compared to the control from serum of Balb/C mice after the treatment with S1NPs and S2NPs for 15 days for dosages of 100–1000 μg/Kg body weight. As shown in Fig. 7a, TNF-α level of S1NPs increased 1.87, 2.48, 3.59, 5.37 folds significantly **(**Fig. 7a**)** and IL-10 level decreased by 1.21, 1.71, 2.13 and 3.77 folds significantly. S2NPs increased the TNF-α level by 1.48, 1.87, 2.58, 3.09 folds but depleted IL-10 level by 1.03, 1.21, 1.50, 1.86 folds **(**Fig. 7**a)**.

The pro and anti-apoptotic protein expression levels after 15 days treatment were enumerated in Table 4, compared to control group. As shown in Fig. 7b-c, both S1NPs and S2NPs displayed likewise increasing trends of the pro-apoptotic protein (Caspases-3, 8, 9) expression level with increase in doses compared to the control. However, the anti-apoptotic expression level of S1NPs and S2NPs (Fig. 7**b-c**) down-regulated in a similar manner for increase in doses. Of note, the up-regulation and down-regulation of S1NPs were higher compared to the S2NPs.

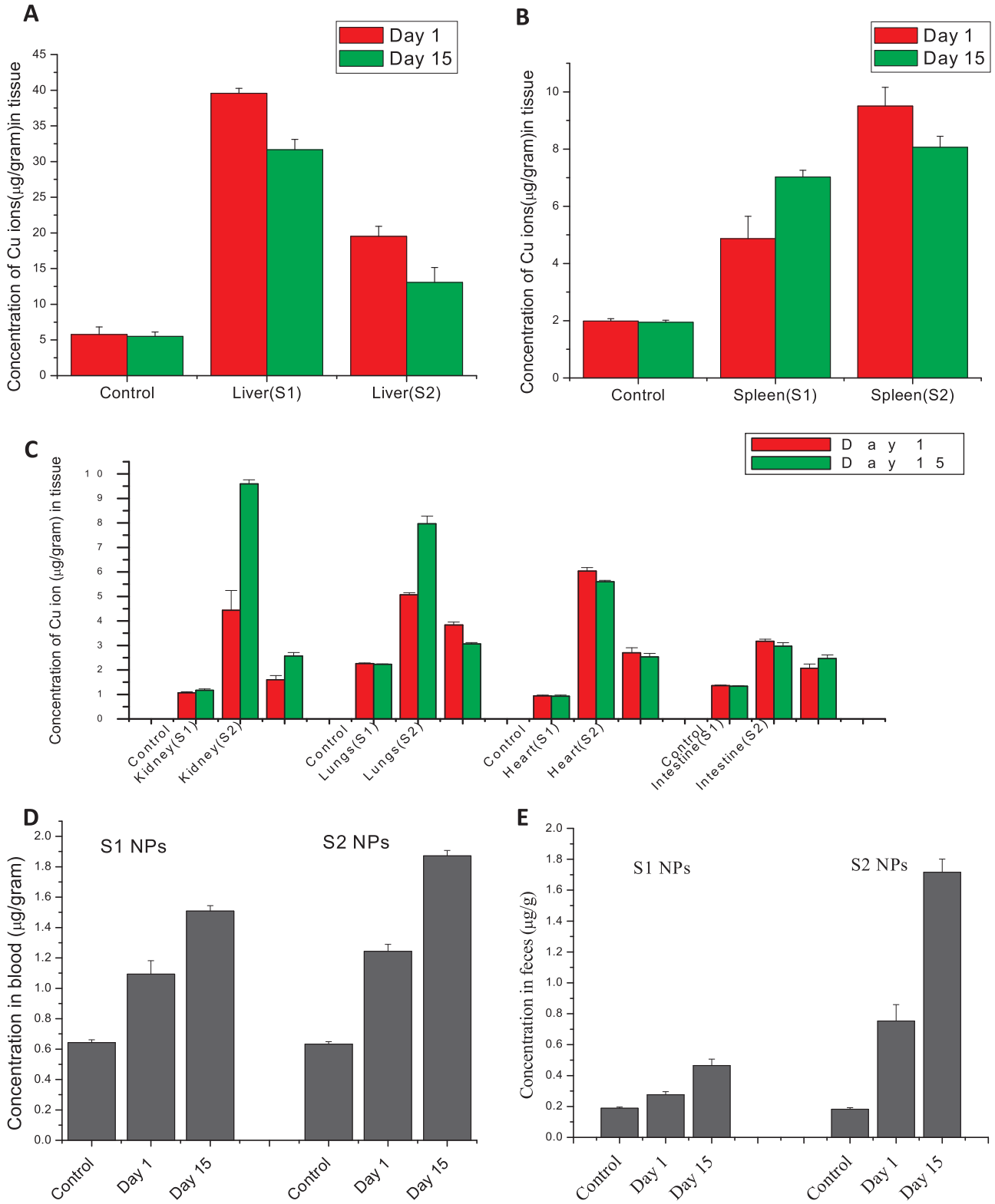

Fig. 6. S1NPs or S2NPs levels in animal tissues, blood and feces as indicators of inorganic NPs biodistribution, circulation and elimination at 1000 μg/mL dose. **(A,B)** Exhibits the contents of **(A)** S1NPs or **(B)** S2NPs in the liver and spleen at both time points. **(C)** Exhibits the contents of S1NPs or S2NPs in the other organs at both time points. **D)** Exhibit concentration of S1NPs and S2NPs in blood. **E)** Concentration of S1 and S2 NPs in feces. Day − 0 to day 15 are the time interval during which the NPs were administered. n = 6. Values are expressed as mean ± SEM; *superscripts indicate significant differences ($P < 0.05$) compared with the control group.

3.3.5. Histopathological study

After 15 days, at 100 μg/ Kg bodyweight S1NPs treated Balb/C mice exhibited minor changes in hepatocytes arrangement. Whereas for 200–1000 μg/Kg bodyweight, disorganization of the hepatocytes, hemocyte overfilling in blood vessels, hepatocyte enlargement, focal lymphocytic infiltration, focal necrosis, diffused vacuolated hepatocytes, loosened liver parenchyma, disarrangement of hepatic lobules, central vein dilation and disruption, were observed (Fig. 8). Whereas

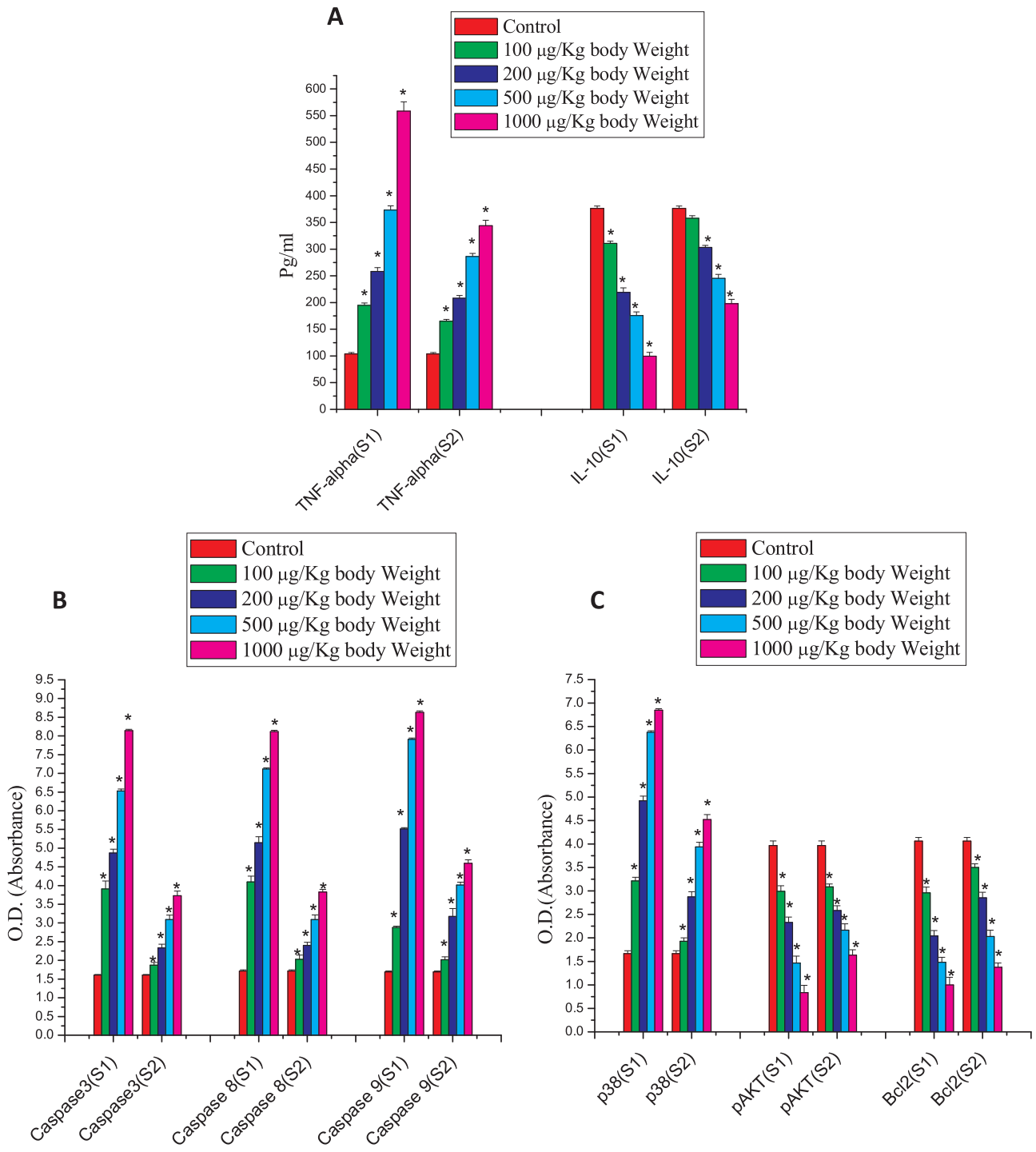

Fig. 7. Cytokines and Apoptotic markers analysis *in vivo*. **(A)** Pro and anti-inflammatory response of S1NPs and S2NPs of mice serum after 15 days (TNF-α, IL-10). **(B,C)** Alteration of pro – apoptotic (Caspase – 8, Caspase – 9, Caspase – 3, p38) and anti – apoptotic (pAKT, Bcl2) response of S1NPs and S2NPs. Values are expressed as mean ± SEM; *superscripts indicate significant differences ($P < 0.05$) compared with the control group.

S2NPs treated mice showed disorganization of the hepatocytes and loosened liver parenchyma but only at higher doses (Fig. 8) (500–1000 µg/Kg bodyweight).

In kidney of S1NPs treated mice, swelling and dilation of Bowman's capsule, deposition of hyaline-like materials in proximal tubules, degeneration changes in epithelium of the proximal tubules as well as rupture of Malpighian corpuscles and Bowman's capsule (Fig. 8) were observed for 100–1000 µg/Kg bodyweight. However in kidney of S2NPs treated experimental group, no significant toxicity was observed for 100–200 µg/Kg bodyweight. Furthermore, in kidney of S2NPs treated experimental group, comparatively lesser swelling of Bowman's capsule and deposition of hyaline-like materials in only some proximal tubules were observed (Fig. 8) for 500–1000 µg/Kg bodyweight. Lastly, disarrangement of proximal tube and rupture

of Bowman's capsule were prominently observed at 1000 µg/Kg bodyweight in S2NPs.

4. Discussion

We successfully synthesized both S1NPs and S2NPs as validated by

Table 4
Estimation of changes in pro and anti-apoptotic markers from mice serum after treatment with S1NPs and S2NPs at different doses (100, 200,500 1000 μg/Kg body weight) for 15 days. Values were expressed as a change in fold compared to control.

Apoptotic Markers	15 Days Different Doses (μg/Kg body weight)			
	100	200	500	1000
Caspase 3 (S1)	2.43	3.04	4.07	5.08
Caspase 8 (S1)	2.39	3.00	4.15	4.74
Caspase 9 (S1)	1.70	3.26	4.68	5.10
P38(S1)	1.93	2.96	3.84	4.12
pAKT(S1)	1.32	1.69	2.71	4.77
Bcl2(S1)	1.4	1.99	2.74	4.06
Caspase 3(S2)	1.23	1.53	2.02	2.45
Caspase 8(S2)	1.38	1.62	2.09	2.59
Caspase 9 (S2)	1.27	2.00	2.53	2.90
P38(S2)	1.14	1.70	2.33	2.69
pAKT(S2)	1.16	1.39	1.71	2.25
Bcl2(S2)	1.12	1.37	1.94	2.86

characterization through SEM, DLS and Zeta potential, FT-IR, AAS before performing *in vitro* and *in vivo* studies.

In our *in vitro* study, we aimed to distinguish the biodistribution and toxicity differences between S1NPs and S2NPs by investigating the Cu ions internalization inside the lymphocytes, biochemical estimation, ROS generation, apoptotic study, pro and anti-apoptotic levels and cytokines estimation. The intracellular concentration of S1NPs was considerably higher compared to S2NPs after administration with 100 μg/mL doses for 24 h in lymphocytes **(**Fig. 2b**)**.

S1NPs and S2NPs toxicity were estimated using human lymphocytes as measured by the MTT and several enzymatic markers. The proportion of viable cells declined after S1NPs or S2NPs exposure compared to control. We observed that % of cell death by S1NPs was higher than S2NPs at all doses, indicating greater cell viability of S2NPs. The higher % of cell death of S1NPs may be attributed to higher intracellular concentration of S1NPs compared to S2NPs. The upstream of various enzymatic (LDH, NADPH and MDA) and non-enzymatic processes implied adverse effects on the cell membrane integrity [38], signal transduction, enzymatic reactions, mitochondrial electron transport chain and gene expression, DNA [39,40] through the generation of ROS [41]. The upstream of enzymatic markers after NPs (S1NPs and S2NPs) exposure suggested significant ROS generation.

Fig. 3**a-b** showed that both S1NPs and S2NPs significantly induced the intracellular production of ROS in human lymphocytes. Overproduction of ROS has been shown to play an important role in oxidative stress through oxidative DNA and protein damage [42]. We observed that S1NPs displayed higher ROS generation levels compared to S2NPs, indicating greater toxicity of S1NPs.

The results presented in Fig. 3**a-d** provided strong evidence that both S1NPs and S2NPs induced apoptosis in lymphocytes with the production of ROS acting as a signaling molecule for the initiation and execution of the apoptotic cell death mechanism [43]. It can be emphasized that S1NPs treated lymphocytes displayed more apoptosis compared to S2NPs. The apoptotic/necrotic study also revealed that S1NPs displayed higher degradation of lymphocytes shape and late apoptosis compared to S2NPs **(**Fig. 3**c-d)**. Previous study demonstrated that, oxidative stress plays a vital role in apoptosis induced by CuONPs in human lung epithelial (A549) cells [4].

In our *in vivo* study, we aimed to distinguish the biodistribution and toxicity differences between S1NPs and S2NPs by examining the body weight, organ weight, organ distribution, biochemistry, histology, pro and anti-apoptotic levels and cytokines estimation. First, we observed reduction of body weight in S1NPs treated mice after intraperitoneal administration for 100–1000 μg/Kg bodyweights after 15 days. Whereas, bodyweight decreased in S2NPs experimental groups only at higher doses (500–1000 μg/Kg bodyweight). We observed mass

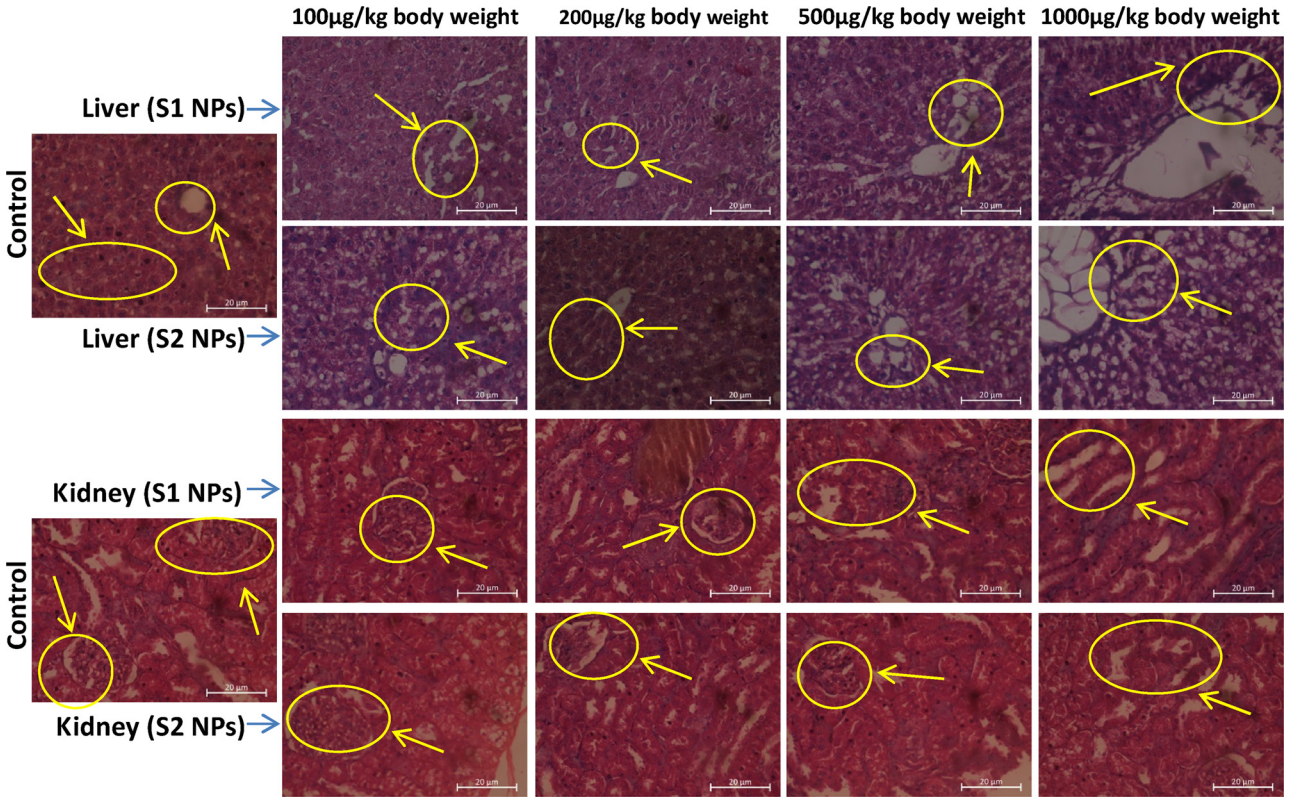

Fig. 8. Histological images of Liver and Kidney. Histological images of hematoxylin-eosin stained Liver and Kidney of Balb/C mice after treatment with different doses (100–1000 μg/mL) of S1NPs and S2NPs after 15 days. The circles in the microscopic image of Liver indicate the areas of leison in liver tissue compared to the control Liver tissue and in case of kidney, the circles indicate histopathological areas of changes due to toxicity compared to the control tissue.

increase in liver and kidney but reduction in spleen weight at all respective dosages. The intraperitoneal exposure of inorganic NPs has been shown to influence the body and organ weight [44]. However, changes in liver, kidney and spleen mass by S1NPs were significantly higher than that of S2NPs. Further, heart mass showed no significant changes in both experimental groups.

At 1000 μg/Kg bodyweight after 15 days, the majority of the S1NPs and S2NPs were accumulated in the liver and spleen. The liver and spleen being part of the mononuclear phagocyte system (MPS), the accumulation could be attributed to the uptake by the phagocytic Kupffer cells in the liver and the macrophages and B cells in the spleen [45–47]. A relatively large amount of S1NPs were accumulated in the kidney, lungs, heart and intestines.

Choi et al. [48] demonstrated that NPs with sizes < 5.5 nm manifested rapid urinary excretion. Hence renal excretion of S1NPs and S2NPs with sizes of 24 ± 6 nm and 44 ± 9 nm respectively could not be the primary route of elimination. Furthermore, significantly higher S2NPs and very few S1NPs were detected in the feces, indicating that the S2NPs but not the S1NPs were excreted through the biliary pathway from the liver to the bile duct, intestine and feces [49].

High levels of TNF-α, induced by NPs act as a regulator of acute inflammation [50]. In our study, the significant dose-dependent up-regulation of pro-inflammatory cytokine TNF-α and down-regulation of anti-inflammatory cytokine IL-10 indicated that both S1NPs and S2NPs increased the inflammatory response, with S1NPs inducing higher inflammatory response *in vitro* and *in vivo*. Similar result was demonstrated by Chattopadhyay et al. [23].

TNF-α triggers apoptosis through activation of initiator caspase, Caspase-8. The Caspase-8 along with the Caspase-9 and 3 mediates mitochondria-operated pathways of apoptosis [51,52]. In the present study, significant up-regulation in the activities of Caspases-3, 8 and 9 and mitogen-activated protein kinase (MAPK) p38 and down-regulation of pAkt and Bcl-2 was observed after S1NPs or S2NPs exposure, indicating that S1NPs and S2NPs induced caspase mediated mitochondrial targeted apoptotic signaling pathways *in vitro* and *in vivo* [53,54]. Our study also found that caspases were more sensitive to S1NPs than S2NPs *in vitro* and *in vivo*.

From the histopathological study we observed significant toxicity in case of S1NPs. After the 15 days treatment with S1NPs, we observed adverse toxicological impact on liver and kidney but S2NPs treated mice showed comparatively less toxicological impact on liver and kidney tissues. Toxicological effects of CuNPs have been shown in kidney, liver and spleen [55] which is in agreement with our present study. Also the dysfunction of liver and kidney as indicated by higher SGOT and creatinine levels of S1NPs and S2NPs reflects the histopathological study.

The NPs morphology, surface functionalization and ion dissolution were major influences in biodistribution and toxicity results of NPs by aiding cellular uptake and translocation of the NPs *in vitro* and *in vivo* [56,57]. Our present study elucidates that, rectangular shaped S1NPs with 26 ± 6 nm diameter significantly killed more normal lymphocytes than spherical shaped S2NPs of 44 ± 9 nm diameters for doses ranging from 1 to 100 μg/mL. The lower toxicity of S2NPs might be attributed to sustained release of S2NPs due to its shape and surface capping agents. Abe et al. [58] demonstrated that the surface modification of CuONPs reduced its toxicity outcomes compared to uncoated CuONPs by precluding intimate contact between cells and NPs. The dissolution of NPs and exertion of toxic ions proved to be susceptible to p^H, composition and exposure time [59]. Previous studies manifested that the surface coating of NPs controlled the composition and structure of the complex protein corona which was formed immediately when NPs were incubated in a biological fluid which was similar to the pathophysiology *in vivo* [60–62]. NPs were stored primarily in the liver and spleen, which then released ions that migrated and accumulated in several major organs [63]. Cho et al. [64] demonstrated that dissolution of metal oxide NPs inside of phagosomes was the main cause of NPs induced toxicity. S1NPs with higher dissolution rates might be responsible for greater toxicity compared to S2NPs particles.

Our present study indicates that green CuONPs is less toxic compared to Chemical CuONPs. Green CuONPs may be used as a drug delivery system and in several biomedical applications in cancer. However further studies involving the beneficial properties of green CuONPs compared to chemical CuONPs are needed to gather valuable information for safety.

5. Conclusion

We demonstrated the *in vitro* and *in vivo* study of S1NPs and S2NPs after their synthesis and physical characterization. The *in vitro* study demonstrated that S1NPs showed more Cu ions internalization and hemolysis than S2NPs in lymphocytes after 24 h. The findings of biochemical markers, ROS generation and apoptosis clearly indicate greater toxicity of S1NPs compared to S2NPs *in vitro*. The *in vivo* study demonstrated that the S2NPs were mainly stored in the liver and spleen, whereas the S1NPs were widely stored in more organs including the heart, lungs, kidney and intestine. The NPs circulation in the blood and excretions in the feces were also found to differ between the S1NPs and the S2NPs. Definite signs of toxicity in mice treated with S1NPs and/or S2NPs were observed over the period of 15 days as indicated by observing the body and organ weight, organ distribution, biochemistry and histology, with S1NPs suggesting greater toxicity than S2NPs. The levels of biomarkers of oxidative stress, apoptosis and cytokines were significantly altered in lymphocytes (after 24 h) and mice serum (after 15 days) treated with both NPs, while more effective change was observed in S1NPs group. These findings suggested that NPs physiochemical compositions (S1NPs and S2NPs) were individually responsible for their distribution and toxicity outcomes *in vitro* and *in vivo*.

Acknowledgement

We are grateful to the Department of Science and Technology(DST) for providing financial assistance to Ms. Aditi Dey through the INSPIRE Fellowship scheme [Grant no. DST/INSPIRE Fellowship/2015/IF 150762]. We are also thankful to the Central Lab of Vidyasagar University (USIC) and University of Calcutta for instrumental support. Special thanks to Mr. Soumik Maiti for his valuable time and effort in editing our manuscript.

Appendix A. Supplementary data

Supplementary material related to this article can be found, in the online version, at doi:https://doi.org/10.1016/j.jtemb.2019.06.012.

References

[1] L.C. Jiang, W.D. Zhang, A highly sensitive nonenzymatic glucose sensor based on CuO nanoparticles-modified carbon nanotube electrode, Biosens. Bioelectron. 25 (2010) 1402–1407.
[2] M.J. Song, S.W. Hwang, D. Whang, Non-enzymatic electrochemical CuO nanoflowers sensor for hydrogen peroxide detection, Talanta 80 (2010) 1648–1652.
[3] F. Perreault, S.P. Melegari, C.H. Da Costa, A.Ld.O.F. Rossetto, R. Popovic, W.G. Matias, Genotoxic effects of copper oxide nanoparticls in Neuro 2A cell cultures, Sci.Total Environ 441 (2012) 117–124.
[4] B. Fahmy, S.A. Cormier, Copper oxide nanoparticles induce oxidative stress and cytotoxicity in airway epithelial cells, Toxicol. In Vitro 23 (2009) 1365–1371.
[5] P. Berntsen, C.Y. Park, B. Rothen-Rutishauser, A. Tsuda, T.M. Sager, R.M. Molina, T.C. Donaghey, A.M. Alencar, D.I. Kasahara, T. Ericsson, E.J. Millet, J. Swenson, D.J. Tschumperlin, J.P. Butler, J.D. Brain, J.J. Fredberg, P. Gehr, E.H. Zhou, Biomechanical effects of environmental and engineered particles on human airway smooth muscle cells, J. R. Soc. Interface 7 (2010) S331–S340, https://doi.org/10.1098/rsif.2010.0068.focus.
[6] M. Yu, Y. Mo, R. Wan, S. Chien, X. Zhang, Q. Zhang, Regulation of plasminogen activator inhibitor-1 expression in endothelial cells with exposure to metal nanoparticles, Toxicol. Lett. 195 (2010) 82–89.

[7] M. Ahamed, M. Karns, M. Goodson, J. Rowe, S. Hussain, J. Schlager, Y. Hong, DNA damage response to different surface chemistry of silver nanoparticles in mammalian cells, Toxicol. Appl. Pharmacol. 233 (2008) 404–410.

[8] M. Salavati-Niasari, F. Davar, Synthesis of copper and copper (I) oxide nanoparticles by thermal decomposition of a new precursor, Mater. Lett. 63 (2009) 441–443.

[9] M. Nasrollahzadeh, Green synthesis and catalytic properties of palladium nanoparticles for the direct reductive amination of aldehydes and hydrogenation of unsaturated ketones, New J. Chem. 38 (2014) 5544–5555.

[10] J.E. Hutchison, Greener Nanoscience: a proactive approach to advancing applications and reducing implications of nanotechnology, ACS Nano 2 (2008) 395–402.

[11] M. Nasrollahzadeh, S.M. Sajadi, M. Maham, Green synthesis of palladium nanoparticles using Hippophaerhamnoides Linn leaf extract and their catalytic activity for the Suzuki–Miyaura coupling in water, J. Mol. Catal. A-Chem. 396 (2015) 297–303.

[12] S.P. Dubey, M. Lahtinen, M. Sillanpää, Tansy fruit mediated greener synthesis of silver and gold nanoparticles, Process Biochem. 45 (2010) 1065–1071.

[13] H.S. Puri, Neem. The Divine Tree (Azadirachta Indica), Harwood academic publishers, Singapore, 1999, pp. 9–21.

[14] E.D. Morgan, Azadirachtin, a scientific gold mine, Bioorg. Med. Chem. 17 (2009) 4096–4105.

[15] R.V. Priyadarsini, R.S. Murugan, P. Sripriya, D. Karunagaran, S. Nagini, The neem limonoids azadirachtin and nimbolide induce cell cycle arrest and mitochondria-mediated apoptosis in human cervical cancer (HeLa) cells, Free Ra dic. Res 44 (2010) 624–634.

[16] M. Geiser, B. Rothen-Rutishauser, N. Kapp, S. Schürch, W. Kreyling, H. Schulz, M. Semmler, V.I. Hof, J. Heyder, P. Gehr, Ultrafine particles cross cellular membranes by nonphagocytic mechanisms in lungs and in cultured cells, Environ. Health Perspect. 113 (2005) 1555-0.

[17] K. Midander, P. Cronholm, H.L. Karlsson, K. Elihn, L. Möller, C. Leygraf, I.O. Wallinder, Surface characteristics, copper release, and toxicity of nano- and micrometer-sized copper and copper (II) oxide particles: a cross-disciplinary study, Small 5 (2009) 389–399.

[18] A.M. Studer, L.K. Limbach, L. Van Duc, F. Krumeich, E.K. Athanassiou, L.C. Gerber, H. Moch, W.J. Stark, Nanoparticle cytotoxicity depends on intracellular solubility: comparison of stabilized copper metal and degradable copper oxide nanoparticles, Toxicol. Lett. 197 (2010) 169–174.

[19] A. Dey, S. Manna, S. Chattopadhyaya, D. Mondal, D. Chattopadhyaya, A. Raj, S. Das, B.G. Bag, S. Roy, Azadirachta indica leaves mediated green synthesized copper oxide nanoparticles induce apoptosis through activation of TNF-α and caspases signaling pathway against cancer cells, J Saudi Chem Soc. 23 (2019) 222–238.

[20] T. Ghosh, T. Chattopadhyay, S. Das, S. Mondal, E. Suresh, E. Zangrando, D. Das, Thiocyanate and dicyanamide anion controlled nuclearity in Mn, Co, Ni, Cu, and Zn metal complexes with hemilabile ligand 2-benzoylpyridine, Cryst. Growth Des. 11 (2011) 3198–3205.

[21] J. Adhikary, B. Das, S. Chatterjee, S.K. Dash, S. Chattopadhyay, S. Roy, J.W. Chen, T. Chattopadhyay, Ag/CuO nanoparticles prepared from a novel trinuclear compound $[Cu\ (Imdz)_4(Ag(CN)_2)_2]$ (Imdz = imidazole) by a pyrolysis display excellent antimicrobial activity, J. Mol. Struct. 1113 (2016) 9–17.

[22] S. Mohapatra, S.K. Mallick, T.K. Maiti, S.K. Ghosh, P. Pramanik, Synthesis of highly stable folic acid conjugated magnetite nanoparticles for targeting cancer cells, Nanotechnology 18 (2007) 385102.

[23] S. Chattopadhyay, S.K. Dash, S. Tripathy, B. Das, D. Mandal, P. Pramanik, S. Roy, Toxicity of cobalt oxide nanoparticles to normal cells; an in vitro and in vivo study, Chem.-Biol. Interact 226 (2015) 58–71.

[24] R. Majumdar, B.G. Bag, N. Maity, Acacia nilotica (Babool) leaf extract mediated size-controlled rapid synthesis of gold nanoparticles and study of its catalytic activity, Int. Nano Lett. 3 (2013) 53.

[25] B. Das, S. Tripathy, J. Adhikary, S. Chattopadhyay, D. Mandal, S.K. Dash, S. Das, A. Dey, S.K. Dey, D. Das, S. Roy, Surface modification minimizes the toxicity of silver nanoparticles: an in vitro and in vivo study, J. Biol. Inorg. Chem. 22 (2017) 893–918.

[26] B. Das, S.K. Dash, D. Mandal, T. Ghosh, S. Chattopadhyay, S. Tripathy, S. Das, S.K. Dey, D. Das, S. Roy, Green synthesized silver nanoparticles destroy multidrug resistant bacteria via reactive oxygen species mediated membrane damage, Arab. J. Chem. 10 (2017) 862–876.

[27] S. Chattopadhyay, S.K. Dash, T. Ghosh, D. Das, P. Pramanik, S. Roy, Surface modification of cobalt oxide nanoparticles using phosphonomethyliminodiaceticacid followed by folic acid: a biocompatible vehicle for targeted anticancer drug delivery, Cancer Nano 4 (2013) 103–116.

[28] L. Hudson, F.C. Hay, Practical Immunology, 3rd edn, Blackwell Pub, Oxford, 1989.

[29] R.A. Heyneman, R.E. Vercauteren, Activation of a NADPH oxidase from horse polymorphonuclear leukocytes in a cell-free system, J. Leukoc. Biol. 36 (1984) 751–759.

[30] S.K. Mahapatra, S.P. Chakraborty, S. Majumdar, B.G. Bag, S. Roy, Eugenol protects nicotine-induced superoxide mediated oxidative damage in murine peritoneal macrophages in vitro, Eur. J. Pharmacol. 623 (2009) 132–140.

[31] S.P. Chakraborty, S.K. Mahapatra, S.K. Sahu, S. Das, S. Tripathy, S. Dash, P. Pramanik, S. Roy, Internalization of Staphylococcus aureus in lymphocytes induces oxidative stress and DNA fragmentation: possible ameliorative role of nanoconjugated vancomycin, Oxid. Med. Cell. Longev. 2011 (2011) 15, https://doi.org/10.1155/2011/942123.

[32] K. Akiyama, C. Chen, D. Wang, X. Xu, C. Qu, T. Yamaza, T. Cai, W. Chen, L. Sun, S. Shi, Mesenchymal-stem-cell-induced immunoregulation involves FAS-ligand-/FAS-mediated T cell apoptosis, Cell Stem Cell 10 (2012) 544–555.

[33] L. Yang, H. Kuang, W. Zhang, Z.P. Aguilar, H. Wei, H. Xu, Comparisons of the biodistribution and toxicological examinations after repeated intravenous administration of silver and gold nanoparticles in mice, Sci. Rep. 7 (2017) 3303.

[34] O.H. Lowry, N.J. Rosenbrough, A.L. Farr, R.J. Randall, Protein measurement with the Folin phenol reagent, J. Biol. Chem. 193 (1951) 265–275.

[35] D. Rehana, D. Mahendirana, S.R. Kumar, A.K. Rahiman, Evaluation of antioxidant and anticancer activity of copper oxide nanoparticles synthesized using medicinally important plant extracts, Biomed. Pharmacother. 89 (2017) 1067–1077.

[36] P. Yugandhar, T. Vasavi, P.U.M. Devi, N. Savithramma, Bioinspired green synthesis of copper oxide nanoparticles from Syzygiumalternifolium (Wt.) Walp: characterization and evaluation of its synergistic antimicrobial and anticancer activity, Appl. Nanosci. 7 (2017) 417–427.

[37] S. Suresh, S. Karthikeyan, K. Jayamoorthy, FTIR and multivariate analysis to study the effect of bulk and nano copper oxide on peanut plant leaves, J. Sci. Adv. Mater. Devices 1 (2016) 343–350.

[38] J.F. Burd, M. Usategui-Gomez, A colorimetric assay for serum lactate dehydrogenase, Clin. Chim. Acta 46 (1973) 223–227.

[39] S. Zhuang, G. Simon, Peroxynitrite-induced apoptosis involves activation of multiple caspases in HL-60 cells, Am. J. Physiol., Cell Physiol. 279 (2000) C341–C351.

[40] S.J. Stohs, D. Bagchi, Oxidative mechanisms in the toxicity of metal ions, Free Radic. Biol. Med. 18 (1995) 321–336.

[41] C. Frädrich, L. Beer, R. Gerhard, Reactive oxygen species as additional determinants for cytotoxicity of Clostridium difficile toxins a and B, Toxins (Basel) 8 (2016) 25, https://doi.org/10.3390/toxins8010025.

[42] W. Droge, Free radicals in the physiological control of cell function, Physiol. Rev. 82 (2002) 47–95.

[43] M. Ott, V. Gogvadze, S. Orrenius, B. Zhivotovsky, Mitochondria, oxidative stress and cell death, Apoptosis 12 (2007) 913–922.

[44] X. Zhang, H. Wu, D. Wu, Y. Wang, J. Chang, Z. Zhai, A. Meng, P. Liu, L. Zhang, F. Fan, Toxicologic effects of gold nanoparticles in vivo by different administration routes, Int. J. Nanomedicine 5 (2010) 771–781.

[45] S. Hirn, M. Semmler-Behnke, C. Schleh, A. Wenk, J. Lipka, M. Schäffler, S. Takenaka, W. Möller, G. Schmid, U. Simon, W.G. Kreyling, Particle size-dependent and surface charge-dependent biodistribution of gold nanoparticles after intravenous administration, Eur. J. Pharm. Biopharm. 77 (2011) 407–416, https://doi.org/10.1016/j.ejpb.2010.12.029.

[46] Y. Xue, S. Zhang, Y. Huang, T. Zhang, X. Liu, Y. Hu, Z. Zhang, M. Tang, Acute toxic effects and gender-related biokinetics of silver nanoparticles following an intravenous injection in mice, J. Appl. Toxicol. 32 (2012) 890–899, https://doi.org/10.1002/jat.2742.

[47] G. Sonavane, K. Tomoda, K. Makino, Biodistribution of colloidal gold nanoparticles after intravenous administration: effect of particle size, Colloids Surf. B Biointerfaces 66 (2008) 274–280, https://doi.org/10.1016/j.colsurfb.2008.07.004.

[48] H.S. Choi, W. Liu, P. Misra, E. Tanaka, J.P. Zimmer, B. Itty Ipe, M.G. Bawendi, J.V. Frangioni, Renal clearance of quantum dots, Nat. Biotechnol. 25 (2007) 1165–1170, https://doi.org/10.1038/nbt1340.

[49] N. Khlebtsov, L. Dykman, Biodistribution and toxicity of engineered gold nanoparticles: a review of in vitro and in vivo studies, Chem. Soc. Rev. 40 (2011) 1647–1671, https://doi.org/10.1039/c0cs00018c.

[50] M.A. Fishman, A.S. Perelson, Th1/Th2 differentiation and cross-regulation, Bull. Math. Biol. 61 (1999) 403–436.

[51] H. Kuang, P. Yang, L. Yang, Z.P. Aguilar, H. Xu, Size dependent effect of ZnO nanoparticles on endoplasmic reticulum stress signaling pathway in murine liver, J. Hazard. Mater. 317 (2016) 119–126, https://doi.org/10.1016/j.jhazmat.2016.05.063.

[52] L. Xu, X. Li, T. Takemura, N. Hanagata, G. Wu, L.L. Chou, Genotoxicity and molecular response of silver nanoparticle (NP)-based hydrogel, Int. J. Nanobiotechnology Pharm. 10 (2012) 16, https://doi.org/10.1186/1477-3155-10-16.

[53] V.N. Ivanov, Z. Ronai, p38 protects human melanoma cells from UV-induced apoptosis through downregulation of NF-kappaB activity and Fas expression, Oncogene 19 (2000) 3003–3012 PMID: 10871852.

[54] J. Pan, Q. Chang, X. Wang, Y. Son, Z. Zhang, G. Chen, J. Luo, Y. Yongyi Bi, F. Fei Chen, X. Shi, Reactive oxygen species-activated Akt/ASK1/p38 signaling pathway in nickel compound-induced apoptosis in BEAS 2B cells, Chem. Res. Toxicol. 23 (2010) 568–577.

[55] Z. Chen, H. Meng, G. Xing, C. Chen, Y. Zhao, G. Jia, T. Wang, H. Yuan, C. Ye, F. Zhao, Z. Chai, C. Zhu, X. Fang, B. Ma, L. Wan, Acute toxicological effects of copper nanoparticles in vivo, Toxicol. Lett. 163 (2006) 109–120.

[56] A. Nel, T. Xia, L. Mädler, N. Li, Toxic potential of materials at the nanolevel, Science 311 (2006) 622–627.

[57] M. Kang, C.H. Lim, J.H. Han, Comparison of toxicity and deposition of nano-sized carbon black aerosol prepared with or without dispersing sonication, Toxicol. Res. 29 (2013) 121–127.

[58] S. Abe, N. Iwadera, T. Narushima, Y. Uchida, M. Uo, T. Akasaka, Y. Yawaka, F. Watari, T. Yonezawa, Comparison of biodistribution and biocompatibility of gelatin-coated copper nanoparticles and naked copper oxide nanoparticles, e-J. Surf. Sci. Nanotech 10 (2012) 33–37.

[59] T. Xia, M. Kovochich, M. Liong, L. Mädler, B. Gilbert, H. Shi, J.I. Yeh, J.I. Zink, A.E. Nel, Comparison of the mechanism of toxicity of zinc oxide and cerium oxide nanoparticles based on dissolution and oxidative stress properties, ACS Nano 2 (2008) 2121–2134.

[60] S. Tenzer, D. Docter, J. Kuharev, A. Musyanovych, V. Fetz, R. Hecht, F. Schlenk, D. Fischer, K. Kiouptsi, C. Reinhardt, K. Landfester, H. Schild, M. Maskos, S.K. Knauer, R.H. Stauber, Rapid formation of plasma protein corona critically affects nanoparticle pathophysiology, Nat. Nanotechno l 8 (2013) 772–781, https://

doi.org/10.1038/nnano.2013.181.
[61] A. Jedlovszky-Hajdú, F. Baldelli Bombelli, M.P. Monopoli, E. Etelka Tombácz, K.A. Dawson, Surface coatings shape the protein corona of SPIONs with relevance to their application in vivo, Langmuir 28 (2012) 14983–14991, https://doi.org/10.1021/la302446h.
[62] U. Sakulkhu, M. Mahmoudi, L. Maurizi, J. Salaklang, H. Hofmann, Protein corona composition of superparamagnetic iron oxide nanoparticles with various physico-chemical properties and coatings, Sci. Rep. 4 (2014) 5020, https://doi.org/10.1038/srep05020.
[63] C.K. Su, H.T. Liu, S.C. Hsia, Y.C. Sun, Quantitatively profiling the dissolution and redistribution of silver nanoparticles in living rats using a knotted reactor-based differentiation scheme, Anal. Chem. 86 (2014) 8267–8274, https://doi.org/10.1021/ac501691z.
[64] W.S. Cho, R. Duffin, S.E. Howie, C.J. Scotton, W.A. Wallace, W. Macnee, M. Bradley, I.L. Megson, K. Donaldson, Progressive severe lung injury by zinc oxide nanoparticles; the role of Zn2+ dissolution inside lysosomes, Part. Fibre Toxicol. 8 (2011) 27, https://doi.org/10.1186/1743-8977-8-27.